International Journal of Innovative
Computing, Information and Control
Volume 8, Number 12, December 2012
 ISSN 1349-4198
pp. 8165–8180

DETECTION OF FALSIFIED FACE USING MOTION INFORMATION

Chih-Chang Yu[1], Chia-Ming Wang[2], Hsu-Yung Cheng[2]
and Kuo-Chin Fan[2]

[1]Department of Computer Science and Information Engineering
Vanung University
No. 1, Van-Nung Rd., Chung-Li, Taoyuan 32061, Taiwan
tacoyu@mail.vnu.edu.tw

[2]Department of Computer Science and Information Engineering
National Central University
No. 300, Jhongda Rd., Jhongli City, Taoyuan 32001, Taiwan
chia@fox1.csie.ncu.edu.tw; {chengsy; kcfan}@csie.ncu.edu.tw

Received September 2011; revised February 2012

Abstract. *This study proposes a system for detecting falsified faces such as photographs of faces and masks by incorporating motion information in face verification and recognition systems. To enhance the robustness of the falsification detection system, a multi-frame optical flow method, which generates significant differences between the optical fields of true faces and that of falsified faces, is adopted. After the optical flow fields are obtained, two classification schemes are applied in the detection system to distinguish true faces and falsified faces, and their results compared. Under the specified motions of true faces and falsified faces, the proposed method can detect falsification with high accuracy. Even when the motion is arbitrary, the proposed system provides satisfying results.*
Keywords: Face falsification detection, Multiple frame optical flow, Motion analysis

1. **Introduction.** Biometric verification systems utilize the physiological and behavioral characteristics of humans to verify their identities. Since the face is one of the most prominent features of a human being, face recognition and verification have been applied in a wide range of biometric verification applications [1]. Generally, the research on face verification falls in two categories. One category includes the use of static information about human faces, neglecting facial expressions and motions. The other involves dynamic information, including that concerning facial expressions, blinking or lip motions. A simple face falsification scheme that uses photographs of faces has been shown to pass a face verification system that uses only static information [2]. This problem is crucial to such applications as ATM security. Since a person might intentionally disguise himself to deceive the verification system and perform unlawful activities, the prevention of such falsification is an important issue to be resolved. However, few researchers have provided solutions to this issue. In the past, IR-based methods have been proposed to solve this problem [2]. Hirayama et al. [2] proposed a method for distinguishing the true faces and photographs thereof based on stereo-photometry. By checking the curvature of IR images, the method can detect curved photographs as well as flat ones. This system [2] does not achieve high accuracy and needs to be improved. Tsuda et al. [3] tried to achieve the same goal using an illumination difference image which is captured using lights from right and left sides. The classification accuracy achieved in the latter work [3] was high for a very small number of testing samples, but the accuracy is not guaranteed when the

dataset is large. Additionally, this method requires that multiple infrared cameras be set up, increasing the cost to an extent that limits practical applications.

This work proposes a framework for solving the problem of detecting possible face falsification with one single camera. Dynamic information about human faces is exploited to improve the discrimination among true faces and falsified faces. The 3D shapes of human faces obviously differ from the photographs of the same faces, resulting in different motion fields in front of the camera. No facial motion, such as blinking or movement of the lip, is present in a photograph: only a real face can move in such a way. To obtain dynamic information about true human faces, optical flow features are adopted herein. Optical flow has been extensively used to represent motion information in various applications [4]. Kruizinga and Petkov [5] proposed an optical flow-based method for face recognition. Kruizinga and Petkov's used compensated residues of optical flow, which convey the difference between one face image and the next image across its optical flow field. Liu et al. [6] proposed an eigenflow method for constructing the optical flow subspace of each human identity. Another approach – the wavelet-based optical flow method [7] was proposed to calculate the consecutive optical flow fields of a sequence of face images. The flow vector across a sequence of frames is then adopted as the feature vector, which contains the spatial and temporal information of human faces. This work develops an optical flow based method that uses both local and global information to estimate face motion for detecting the falsification of faces.

The two well-known methods for solving optical flow problems are the Horn-Schunck method [8] and the Lucas-Kanade method [9]. In the Horn-Schunck method, the assumed smoothness constraint that is adopted into the optical flow estimation is that the gradient of optical flow does not change abruptly in the spatial domain. Hence, the Horn-Schunck method finds the optical flow that minimizes the square of the magnitude of the optical flow gradient. Many methods of iteratively solving linear motion constraint equations have been proposed. They include Gauss-Seidel relaxation, successive over-relaxation and local relaxation [10]. For non-linear motion constraint equations, Kim [11] proposed a nonlinear relaxation approach. However, the global constraint used in Kim's work [11] is very sensitive to noises. Another frequently used method is Lucas-Kanade method [9]. It assumes that all points in a small patch have the same motion. The solution to compute optical flow is formulated as a least-square problem, which has a simple closed-form solution. It is very useful when enough local information is available at each point. However, the method fails when local information is absent in a homogenous region as which the "aperture problem". Bruhn et al. [12] combined both global and local constraints using both Horn-Schunck and Lucas-Kanade methods. However, their approach is very time consuming because it must be solved iteratively. Another way to improve the accuracy of flow estimation is to use more frames to constrain the optical flow components. Bergen et al. [13] proposed a three-frame method to analyze multiple motions within a small region. Shariat [14] presented a method for computing three-dimensional motion parameters by finding the correspondence of the same point in five frames. However, the numbers of image points that can be used for calculating optical flow are limited. Irani [15] proposed a multi-frame optical flow estimation method using subspace constraints. She reported that all points across multiple frames commonly reside in a low-dimensional subspace, and her method required no prior model of camera or scene. However, the optical flows of all image points are estimated simultaneously using an iterative procedure, increasing the computational complexity higher. In this work, multiple frames are used to increase the stability of considering local information and enforce a temporal smoothness of flow fields to estimate the real global motion. Since the estimation noise can be reduced by the multi-frame optical flow method, this method

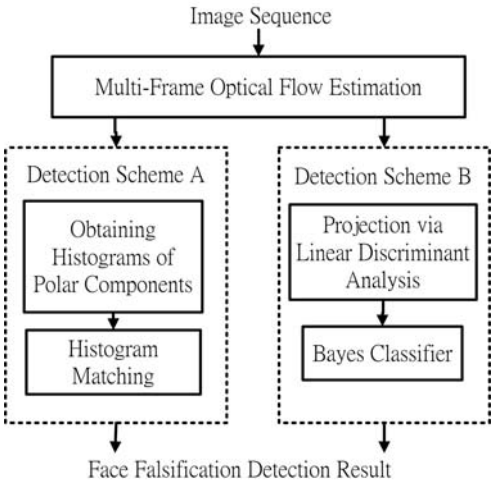

FIGURE 1. Block diagram of proposed system

distinguishes the difference between the flow fields of true faces and photographs of faces more easily than traditional optical flow methods. Also, an estimation method with closed-form solutions is favored to reduce computational complexity. Figure 1 presents a block diagram of the proposed framework. After the multi-frame optical flow fields are obtained, two detection schemes using the estimated flows as features are implemented. They are compared herein. The first scheme converts the flow estimation results into polar components and uses histogram matching to distinguish true faces from falsified faces. The second projects the dense optical flow field across a short period of time into an optimal subspace using Linear Discriminant Analysis (LDA) [16] and utilizes a Bayesian classifier to perform classification [17].

The rest of the paper is organized as follows. Section 2 explains the proposed multi-frame optical flow estimation. Section 3 elucidates the two face falsification detection schemes. Section 4 presents the experimental results that verify the effectiveness of the proposed multi-frame optical flow estimation and detection system. Finally, Section 5 concludes the paper.

2. **Multi-frame Optical Flow Estimation.** The proposed optical flow estimation method is implemented using integrating multiple image frames so that the flow field is simultaneously constrained in both time and spatial domains. Let $I^i(x, y)$ be the image function at time i and (u, v) be the optical flow from I^0 to I^1. The brightness constancy equation states that $I^0(x-u,y-v) = I^1(x, y)$. When (u, v) are very small, $I^0(x-u, y-v)$ can be linearized by Equation (1).

$$I^0(x - u, y - v) \approx I^0(x, y) - uI_x^0 - vI_y^0 \tag{1}$$

The image flow constraint equation can be derived using the first-order Taylor expansion.

$$uI_x^0 + vI_y^0 + I_t^0 = 0 \tag{2}$$

where $I_t^0 = I^1(x, y) - I^0(x, y)$ is the derivative with respect to time of I^0 and (I_x^0, I_y^0) is the spatial gradient of I^0. Equation (2) approximates the brightness constancy of one point. Since Equation (2) alone cannot be solved for the two variables (u, v), more constraints are needed.

The proposed multi-frame extension method is implemented based on the derivation of the image flow constraint equation in a local patch across a sequence of frames. In estimating the optical flow of a certain point, T frames before and after the reference

frame are considered. Let I^j be the image frame at time j, $x_i = [x_i, y_i]$ be the spatial coordinates of point i, and I^0 be the reference image which is used to estimate the optical flow. In the image sequence before and after the reference frame, the difference between adjacent frames from time $-T$ to T is accumulated and minimized to optimize (u, v). The error function is

$$\varepsilon(\boldsymbol{\alpha}_i) = \sum_{j=-T}^{T-1} \sum_{k \in \Omega_i} \left[I^{j+1}\left(T(\mathbf{x}_k; \boldsymbol{\alpha}_i, j+1)\right) - I^j\left(T(\mathbf{x}_k; \boldsymbol{\alpha}_i, j)\right) \right]^2 \tag{3}$$

where Ω_i is the neighborhood of point i. In Equation (3), the term in parentheses is the error sub-term between frames j and $j+1$ and is denoted $\varepsilon_{j,j+1}$. Here, α_i are the motion parameters of various motion models. In the system, human faces are assumed to move with constant velocity in a short period, and α_i is taken as the parameter of the constant model. Suppose that the amount of optical flow at each point is very small, under the constant model assumption, $\varepsilon_{j,j+1}$ can be rewritten as a first-order Taylor expansion,

$$\varepsilon_{j,j+1} = u_i \left((j+1) I_{x_k}^{j+1} - j I_{x_k}^j \right) + v_i \left((j+1) I_{y_k}^{j+1} - j I_{y_k}^j \right) + I^{j+1}(\mathbf{x}_k) - I^j(\mathbf{x}_k) \tag{4}$$

To minimize the error function, for each point i, partial derivatives are obtained as in Equation (5).

$$\begin{aligned} 0 = \frac{\partial \varepsilon}{\partial \mathbf{v}_i} = \begin{bmatrix} \frac{\partial \varepsilon}{\partial u_i} \\ \frac{\partial \varepsilon}{\partial v_i} \end{bmatrix} = & \begin{bmatrix} \sum_{j=-T}^{T-1} \sum_{k \in \Omega_i} (Iinc_{x_k}^j)^2 & \sum_{j=-T}^{T-1} \sum_{k \in \Omega_i} (Iinc_{x_k}^j \cdot Iinc_{y_k}^j) \\ \sum_{j=-T}^{T-1} \sum_{k \in \Omega_i} (Iinc_{x_k}^j \cdot Iinc_{y_k}^j) & \sum_{j=-T}^{T-1} \sum_{k \in \Omega_i} (Iinc_{y_k}^j)^2 \end{bmatrix} \begin{bmatrix} u_i \\ v_i \end{bmatrix} \\ & + \begin{bmatrix} \sum_{j=-T}^{T-1} \sum_{k \in \Omega_i} \left(I_{t_k}^j\right) \cdot Iinc_{x_k}^j \\ \sum_{j=-T}^{T-1} \sum_{k \in \Omega_i} \left(I_{t_k}^j\right) \cdot Iinc_{y_k}^j \end{bmatrix} \end{aligned} \tag{5}$$

Finally, the closed-form estimate of the multiple frame optical flow

$$\begin{aligned} \begin{bmatrix} u_i \\ v_i \end{bmatrix} = & \begin{bmatrix} \sum_{j=-T}^{T-1} \sum_{k \in \Omega_i} (Iinc_{x_k}^j)^2 & \sum_{j=-T}^{T-1} \sum_{k \in \Omega_i} (Iinc_{x_k}^j \cdot Iinc_{y_k}^j) \\ \sum_{j=-T}^{T-1} \sum_{k \in \Omega_i} (Iinc_{x_k}^j \cdot Iinc_{y_k}^j) & \sum_{j=-T}^{T-1} \sum_{k \in \Omega_i} (Iinc_{y_k}^j)^2 \end{bmatrix}^{-1} \\ & \begin{bmatrix} -\sum_{j=-T}^{T-1} \sum_{k \in \Omega_i} \left(I_{t_k}^j\right) \cdot Iinc_{x_k}^j \\ -\sum_{j=-T}^{T-1} \sum_{k \in \Omega_i} \left(I_{t_k}^j\right) \cdot Iinc_{y_k}^j \end{bmatrix} \end{aligned} \tag{6}$$

where

$$I_{t_k}^j \equiv I^{j+1}(x_k, y_k) - I^j(x_k, y_k) \tag{7}$$

$$Iinc_{x_k}^j \equiv \left((j+1) \cdot I_{x_k}^{j+1} - j \cdot I_{x_k}^j \right), \quad Iinc_{y_k}^j \equiv \left((j+1) \cdot I_{y_k}^{j+1} - j \cdot I_{y_k}^j \right) \tag{8}$$

From the model formulations, we can derive the closed-form optical flow estimate can be derived. The aforementioned multiple frame optical flow estimation approach is called the "Incremental Difference Approach" (IDA). Our previous work [18] discussed another multiple frame optical flow estimation method called the Reference Frame Approach (RFA), which accumulates the differences between the reference frame image and all other frame images from time $-T$ to T. RFA has a larger error than IDA in the numerical approximation procedure, and therefore IDA outperforms RFA. The IDA method takes into account

more temporal information than does the Lucas-Kanade's method [9]. The merits of the derived IDA optical flow fields are that they are numerically more stable, have less ambiguous matching between adjacent frames, and are smooth with less noise. These characteristics are important because we use the flow field from consecutive frames as the features to detect face falsification. The experimental results below will demonstrate the effectiveness of the proposed IDA optical flow estimation method.

3. **Methods for Face Falsification Detection.** After the optical flow fields have been successfully estimated, two methods for detecting face falsification are implemented. Distinguishing true faces from falsified faces can be regarded as a two-class classification problem. The first scheme converts the flow estimation results into polar components and uses histogram matching to distinguish true faces from falsified faces. The second scheme projects the dense optical flow field across a short period of time into an optimal subspace using Linear Discriminant Analysis (LDA) and utilizes a Bayesian classifier to perform classification. The following two subsections explain these two schemes, whose results are compared in Section 4.

3.1. **Detection scheme A: Extraction of polar component with histogram matching.** This sub-section describes the first scheme for detecting face falsification. Firstly, the polar components, magnitude r and orientation θ, of an optical flow vector (u, v) are obtained using Equations (9) and (10).

$$r = \sqrt{u^2 + v^2} \tag{9}$$

$$\theta = \tan^{-1} \frac{v}{u} \tag{10}$$

Then, histograms are constructed based on the polar components of the optical flow vectors for each motion model. Let B be the universal bin set and b_i be a histogram bin where $b_i \in B$. The histograms are normalized using Equation (11).

$$\tilde{X}_{b_i} = \frac{X_{b_i}}{\sum\limits_{\forall b_i \in B} X_{b_i}}, \quad \forall b_i \in B \tag{11}$$

where $\tilde{X}$ is the normalized histogram of X and all bin values X_b are in the interval $[0, 1]$ after normalization. The L_1 norm is used as a metric of similarity. The histogram-based detection scheme matches the test sample with the template histograms in the database directly. The next sub-section considers a very different approach using a mathematical modeling procedure.

3.2. **Detection scheme B: Linear discriminant analysis (LDA) with Bayesian classifier.** In this detection scheme, $r \times c$ IDA flow fields across F frames are collected and rearranged to a k by 1 vector where $k = r \times c \times F$, to form the training samples. Linear Discriminant Analysis (LDA) is adopted to estimate the projected subspace that best separates two classes of high-dimensional training data. After the successful estimation of projection axis w being, the training samples are projected using $y = w^T x$ and two Gaussians are fitted to the projected data y to obtain the conditional probability densities of the two classes. The Bayesian decision rule, given by Equation (12), is used as the classifier

$$Decision = \begin{cases} \omega_1, & \text{if } p(\omega_1|\mathbf{y}) > p(\omega_2|\mathbf{y}) \\ \omega_2, & \text{otherwise} \end{cases} \tag{12}$$

where $p(\omega_i|y)$ is the posterior probability. For simplicity, the prior probabilities can be assumed to be equal, and thus the posterior probabilities are proportional to the class-conditional probabilities $p(y|\omega_i)$.

4. **Experimental Results.** This section explains the experimental results that verify the feasibility and effectiveness of the proposed system. Data are generated from the true face and photographs of the faces of 12 subjects. Each subject performs two kinds of motion – restricted motion and arbitrary motion – to generate the true face data. The restricted motions are panning left/right and tilting up/down. The duration of the motion sequences of each subject is 300-400 frames. One-half of the data are to be used for training. The others are used for testing. The optical flow information is extracted and a corresponding histogram is established for each motion sequence.

TABLE 1. Average number of ambiguous matching points of three Benchmark sequences

Method	The Yosemite sequence 79632 pixels/frame		The Rubik's Cube sequence 61440 pixels/frame		The Nasa sequence 90000 pixels/frame	
	Average number of ambiguous points	Percentage of ambiguous points	Average number of ambiguous points	Percentage of ambiguous points	Average number of ambiguous points	Percentage of ambiguous points
Lucas-Kanade	4192	5.3%	21753	35.4%	4272	4.7%
IDA- 3 frames	370	0.5%	7813	12.7%	3438	3.8%
IDA- 4 frames	84	0.1%	5512	9.0%	3285	3.6%
IDA- 5 frames	30	0.04%	5350	8.7%	3104	3.4%
IDA- 6 frames	9	0.01%	5282	8.6%	3014	3.3%
IDA- 7 frames	1	0.00%	5214	8.5%	2884	3.2%

(a) Original image frames of true faces

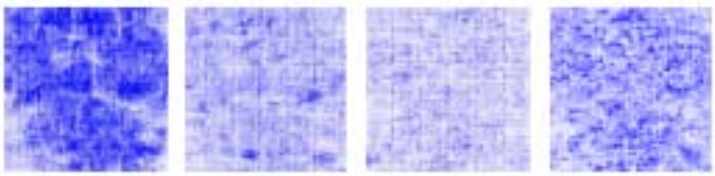

(b) IDA (c) Lucas-Kanade (d) Horn-Schunck (e) Irani

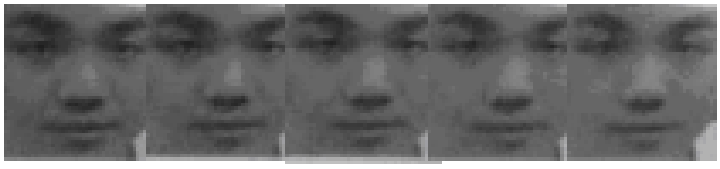

(f) Original image frames of falsified faces

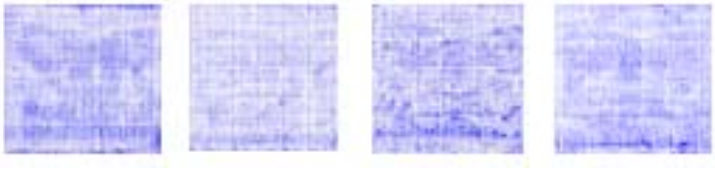

(g) IDA (h) Lucas-Kanade (i) Horn-Schunck (j) Irani

FIGURE 2. Optical flows of true faces and falsified faces using different estimation methods

Firstly, the advantages of the proposed IDA optical flow over traditional optical flow estimation method are demonstrated. Table 1 summarizes the average number of ambiguous points using three different benchmark sequences: the Yosemite sequence, the Rubik's Cube sequence and the Nasa sequence. As shown in Table 1, the number of ambiguous points drops as more frames are considered in the IDA method. The proposed IDA method greatly alleviates the problem of ambiguous matching related to the Lucas-Kanade's method [9], which results in up to 35% ambiguous points in the Rubik's Cube sequence. Hence, the estimation of flow field using the proposed IDA method is more accurate. Figure 2 shows the flow fields of the panning motion of a true face (Figure 2(a)) and a falsified face (Figure 2(f)). From Figures 2(b) and 2(d), the differences between the IDA optical flow fields of the true face and the falsified face are obvious. Figures 2(c)-2(e) display the optical flow estimation results of the true face using the Lucas-Kanade method, the Horn-Schunck method, and the Irani's methods, respectively. Comparing Figures 2(c)-2(e) with their corresponding optical flow estimation results of the face photographs in Figures 2(h)-2(j), differences that are not as apparent as those demonstrated using the IDA method. This experiment reveals the benefits of employing IDA in the detection of face falsification. Figure 3 shows the differences between the IDA optical flows of true faces and falsified faces that are performing panning and tilting motions.

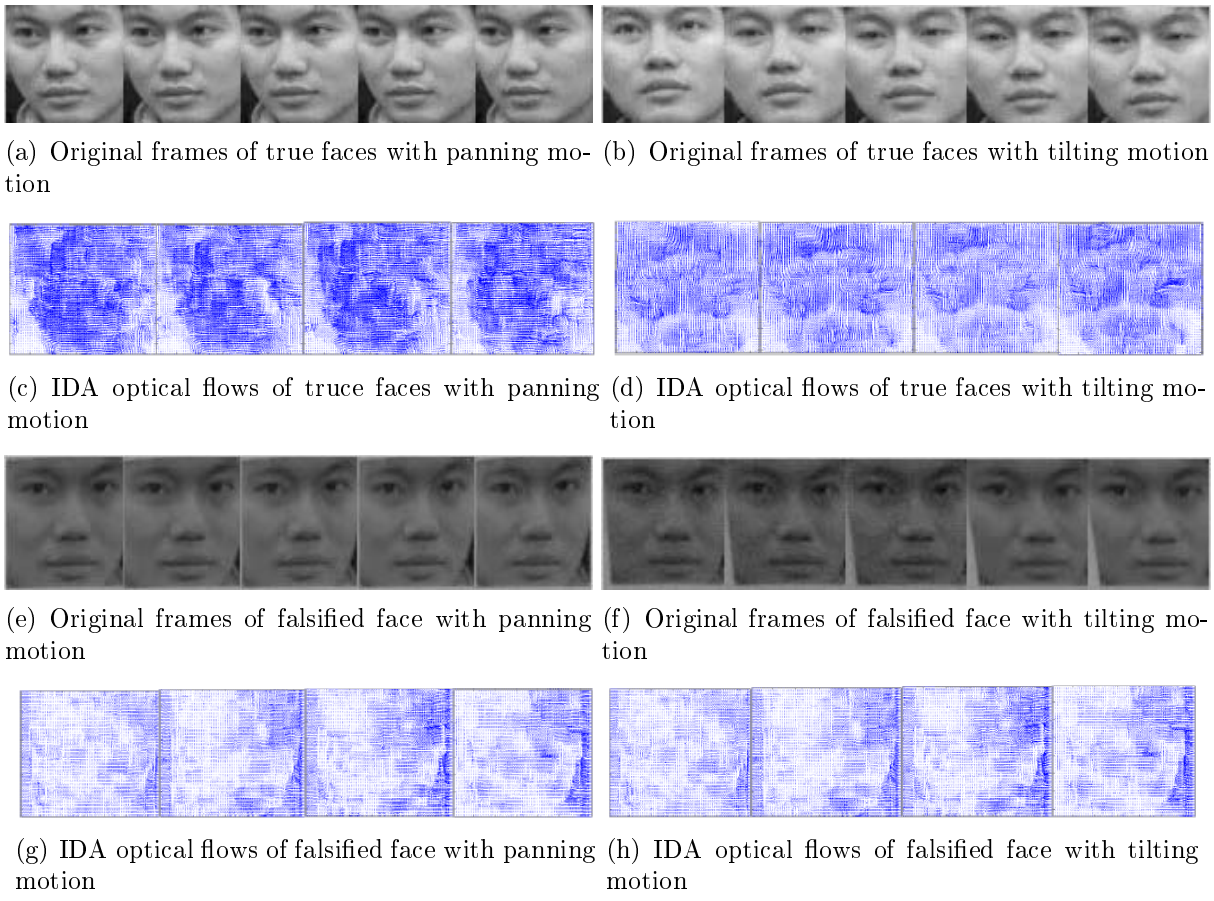

(a) Original frames of true faces with panning motion

(b) Original frames of true faces with tilting motion

(c) IDA optical flows of truce faces with panning motion

(d) IDA optical flows of true faces with tilting motion

(e) Original frames of falsified face with panning motion

(f) Original frames of falsified face with tilting motion

(g) IDA optical flows of falsified face with panning motion

(h) IDA optical flows of falsified face with tilting motion

FIGURE 3. IDA optical flows of true faces and falsified faces: (a), (b) original image sequences of true faces with panning and tilting motions; (c), (d) optical flows of (a) and (b); (e), (f) original image sequences of falsified faces with panning and tilting motions; (g), (h) optical flows of (e) and (f)

Figure 3 confirms the distinguish ability between the IDA flows of true faces and those of falsified faces.

The second experiment involves the histogram-based detection scheme elucidated in Subsection 3.1. In this experiment, the motion of the users' face is restricted to panning and tilting. One histogram is constructed based on the polar components of the optical flow vectors for each model of the true faces and the falsified faces. Four motion models, pan-right, pan-left, tilt-up and tilt-down, are considered in this experiment. Figure 4 illustrates the histograms of the four motion models of the true faces, and Figure 5 shows those of the falsified faces. Table 2 lists the results of falsification detection by the proposed detection scheme for different numbers of frames and histogram bins. Generally, as fewer frames are used, the flow noise increasingly tends to dominate the sample and reduce the detection accuracy. The bin number does not significantly influence the performance when the number of bins is larger than 60. The precision rate of this falsification detection scheme can reach 98.51%, and higher if more frames are used. However, the recall rates are all below 80%, which is not satisfactory. Therefore, another detection scheme that is based on Linear Discriminant Analysis and Bayesian classifier is considered.

The third experiment is designed to verify the classification mechanism that was described in Subsection 3.2. As stated in Subsection 3.2, flow fields across F frames are collected to form a sample and then each sample is projected to the optimal subspace using the projection axis that is computed by LDA. As the black bars in Figure 6(a) show, the features of the true faces after projection are normally distributed in space with a small variance. The distribution of falsified face after projection also forms a normal-like distribution, but with a larger variance, indicated by the white bars in Figure 6(a). Therefore, two Gaussians are used herein to model the projection distributions of the two classes. Figure 6(b) shows the two Gaussians that are fitted onto the projected distribution. The true face data are modeled by the Gaussian with solid line.

Figure 7 shows the results of projecting test data; the 'Asterisk' markers to represent true face samples; the 'circle' markers to represent falsified face samples, and the straight line denotes the decision boundary. First the users' motion is restricted to be panning and tilting motions only. Table 3 tabulates the results of falsification detection. In this experiment, the number of frames F used for one sample ranges from five to nine. From the experiment results, the information that is embedded in the optical flow field across a period is effective in distinguishing true faces from falsified faces. Both precision and recall rates are higher than 95% for the LDA and Bayesian Classifier based detection scheme. The precision and recall rates slightly increase with the number of frames that are used to form the feature vector. If the restrictions of panning and tilting motions are relaxed and arbitrary face motions are allowed, then the projected test data become more cluttered, as shown in Figure 8, and the resulting falsification detection rates are therefore lower, as listed in Table 4. However, the precision and recall rates remain around 90%

TABLE 2. Detecting falsification using histogram-based detection scheme considering different numbers of frames and numbers of bins

Number of frames	30 Bins		60 Bins		90 Bins		180 Bins	
	Precision	Recall	Precision	Recall	Precision	Recall	Precision	Recall
5 Frames	89.21%	68.45%	90.99%	70.83%	90.99%	70.83%	90.99%	70.83%
6 Frames	98.84%	65.47%	97.80%	68.35%	97.80%	68.35%	97.80%	68.35%
7 Frames	95.02%	68.75%	95.20%	71.43%	95.14%	70.54%	95.14%	70.54%
8 Frames	95.72%	73.74%	97.18%	75.76%	97.18%	75.76%	97.18%	75.76%
9 Frames	98.43%	77.01%	98.51%	79.31%	98.51%	79.31%	98.51%	79.31%

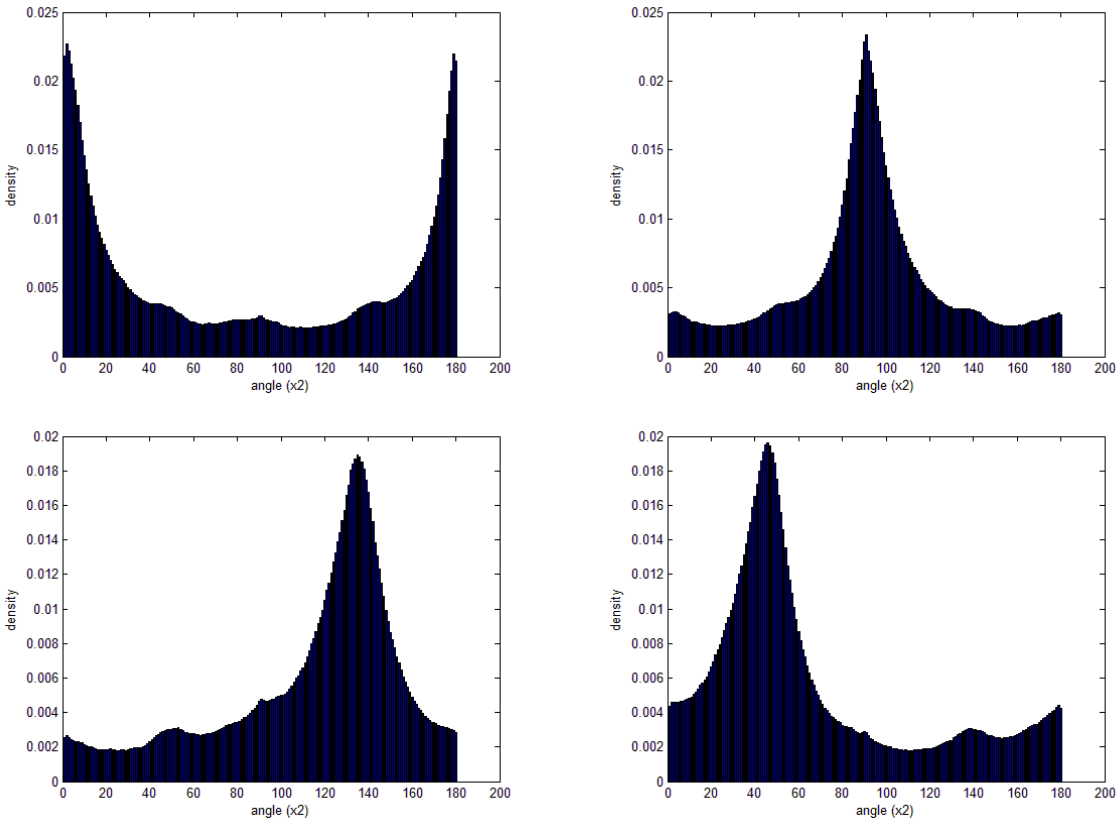

(a) Histograms with 180 bins

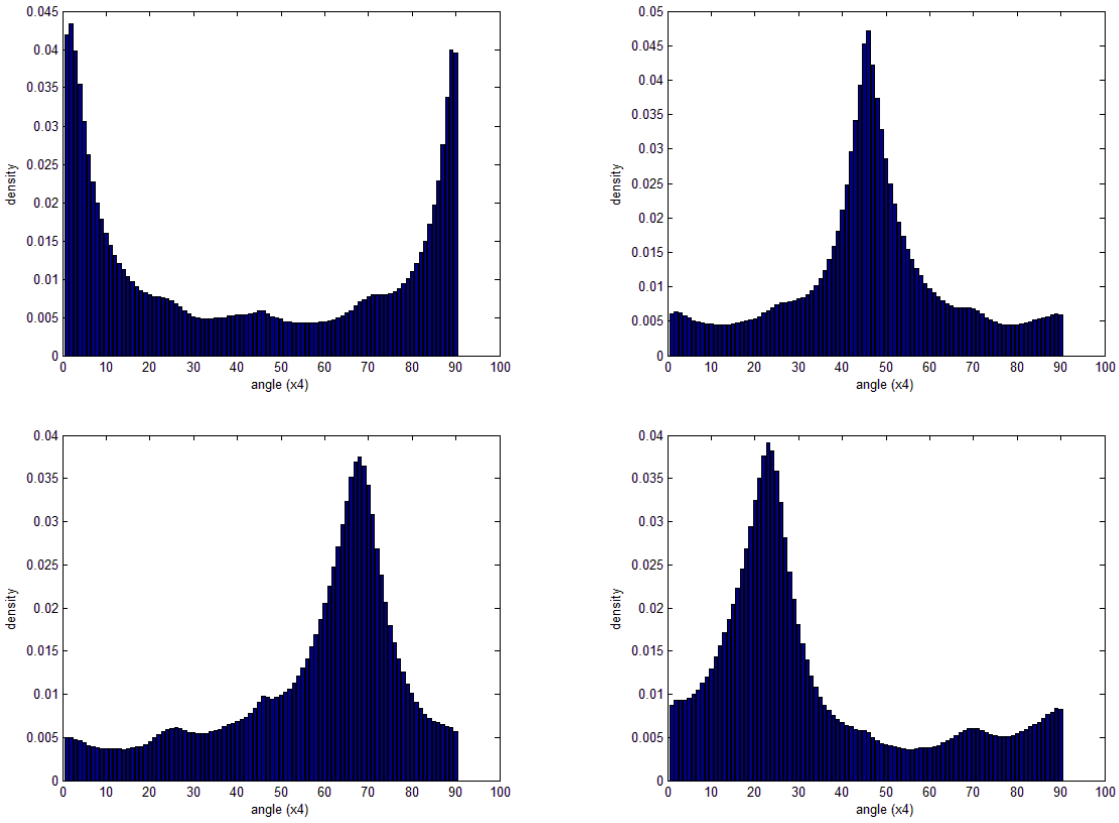

(b) Histograms with 90 bins

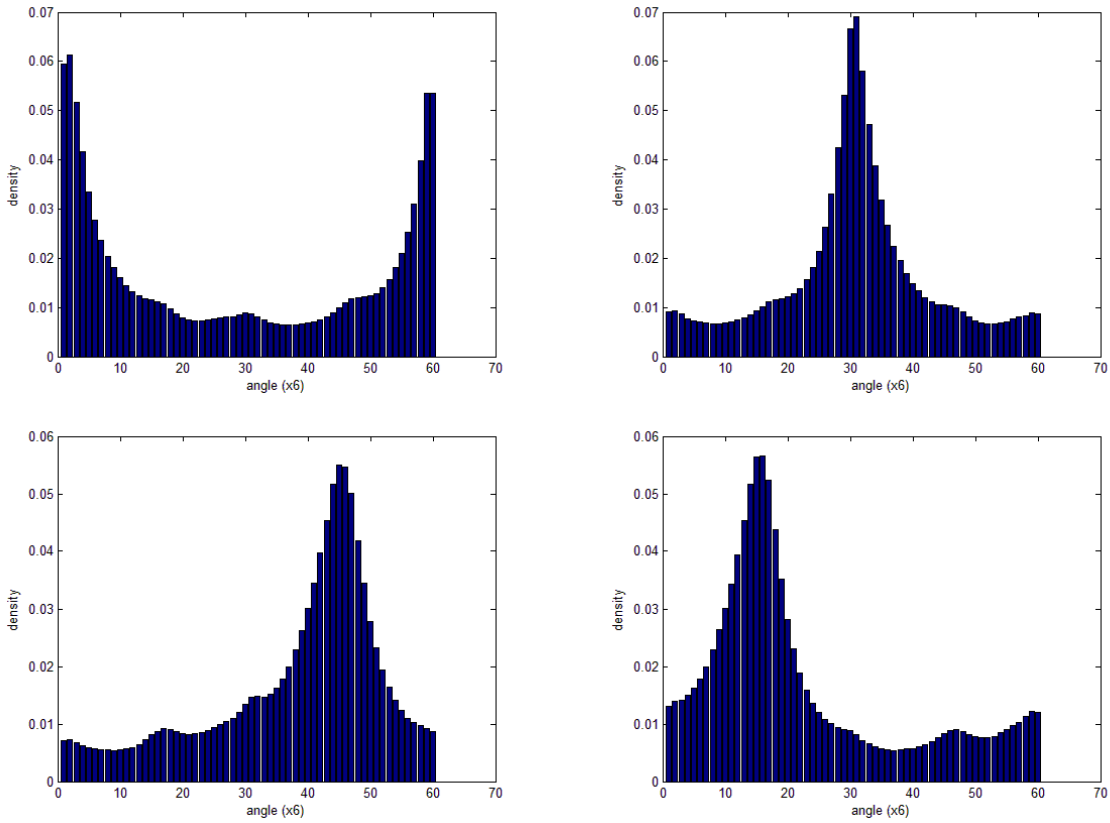

(c) Histograms with 60 bins

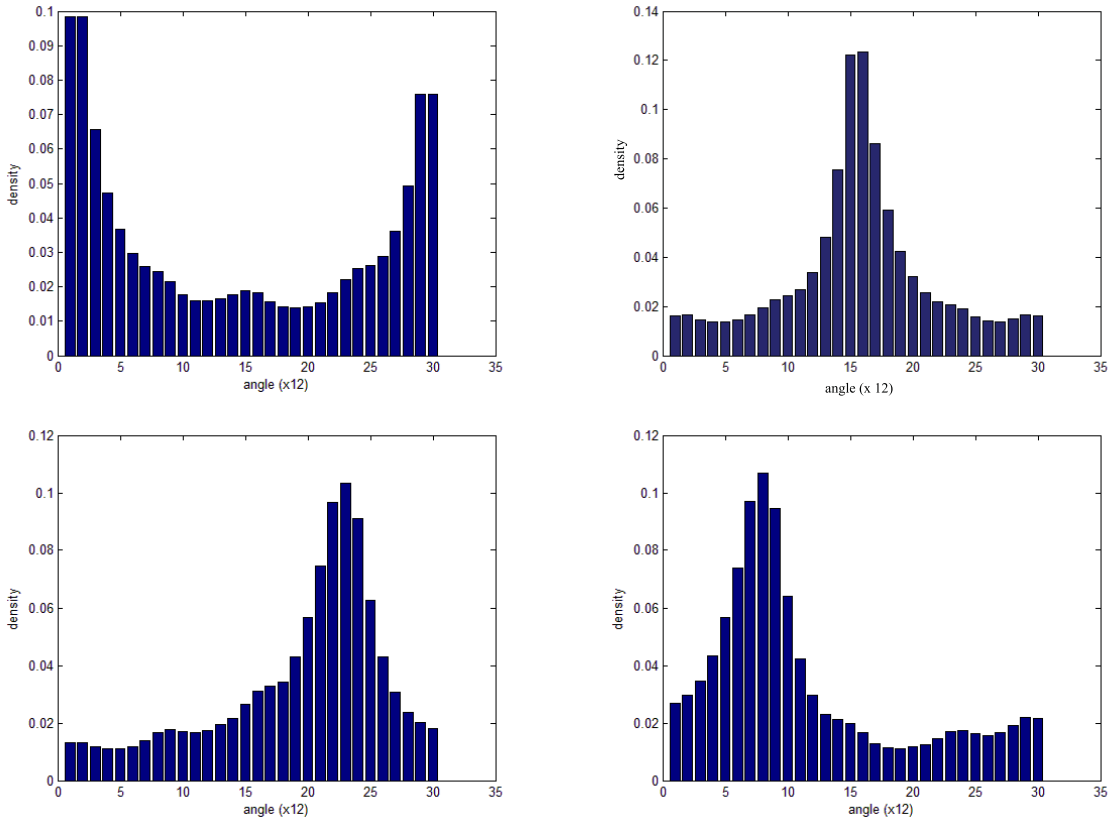

(d) Histograms with 30 bins

FIGURE 4. Histograms for the four different motion models (pan left, pan right, tilt up and tilt down) of the true faces with various number of bins

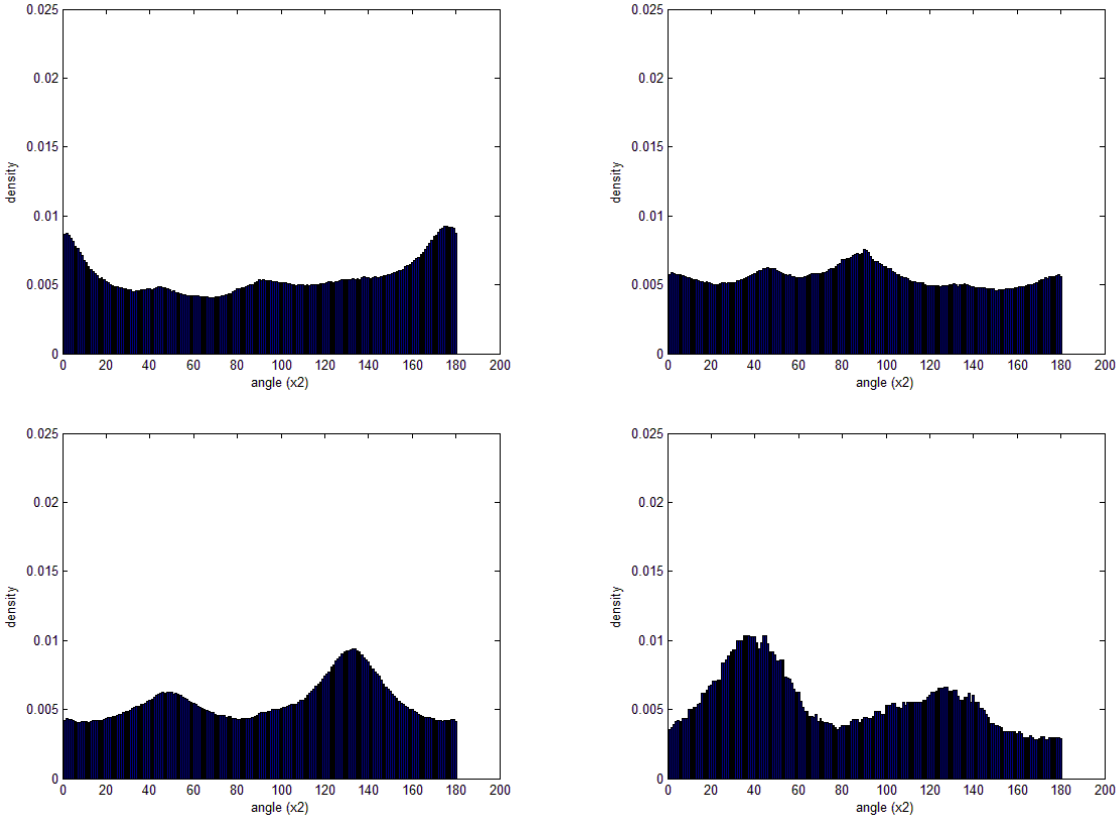

(a) Histograms with 180 bins

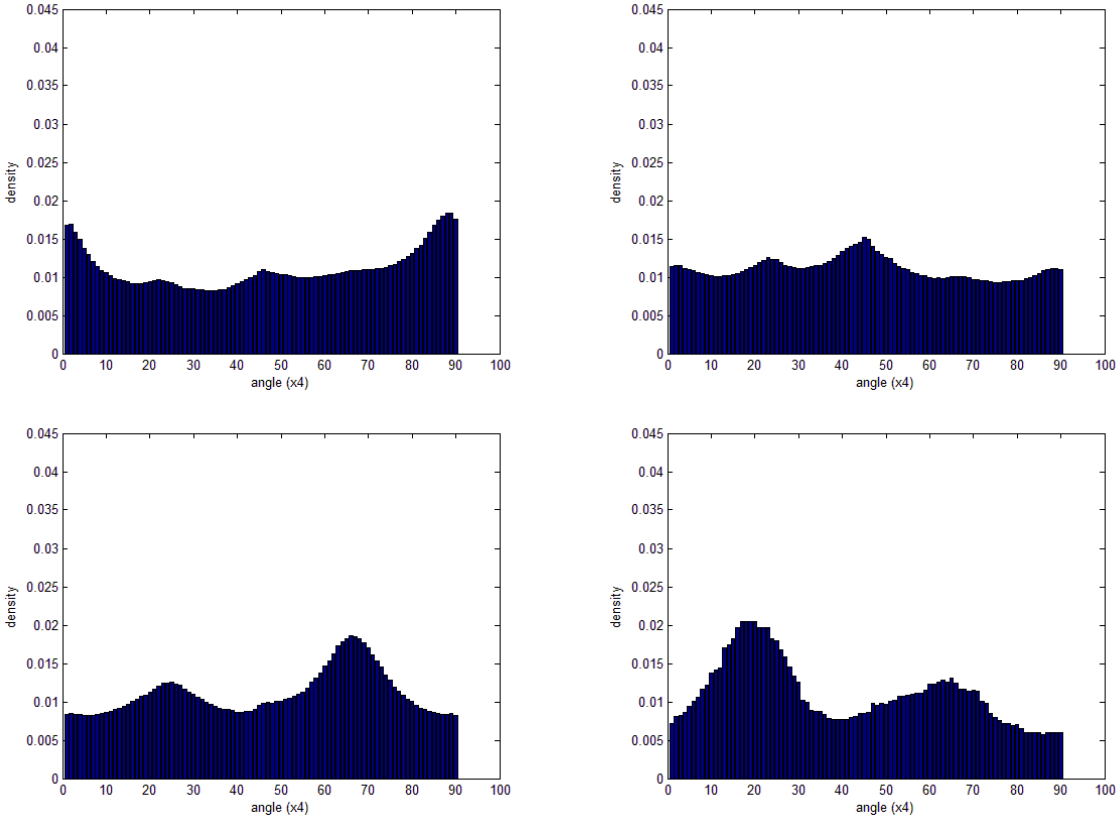

(b) Histograms with 90 bins

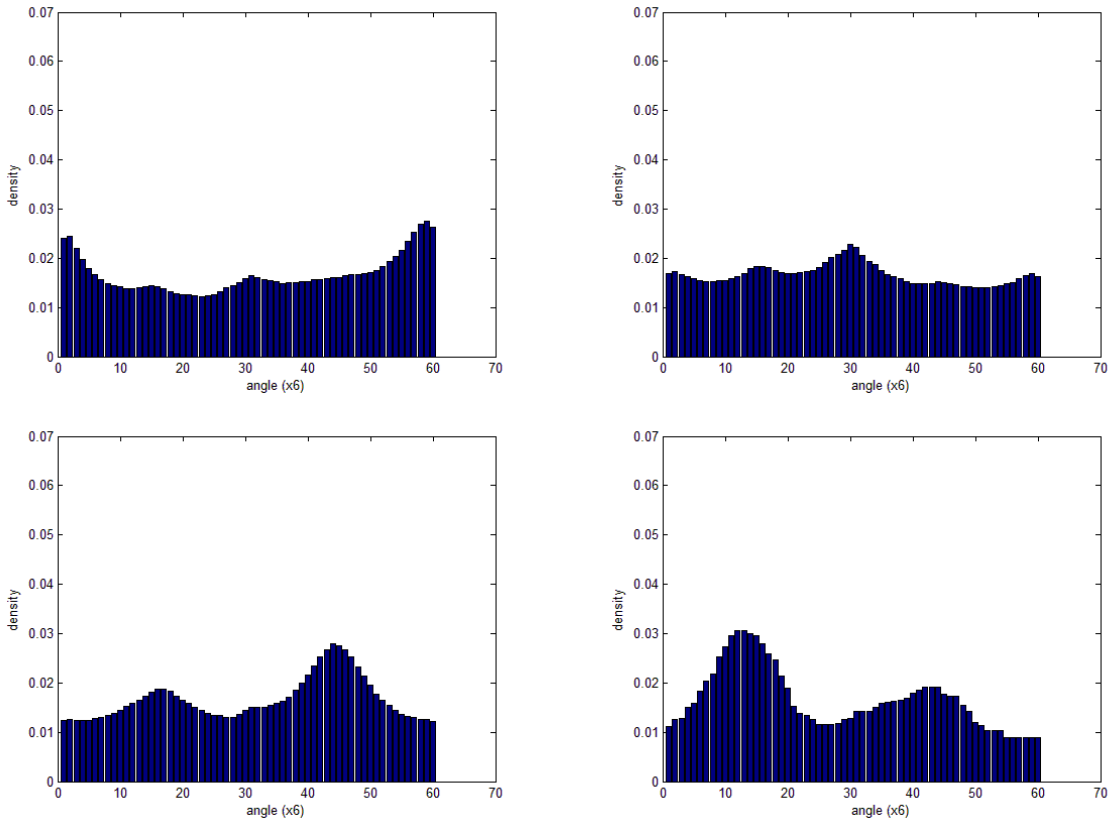

(c) Histograms with 60 bins

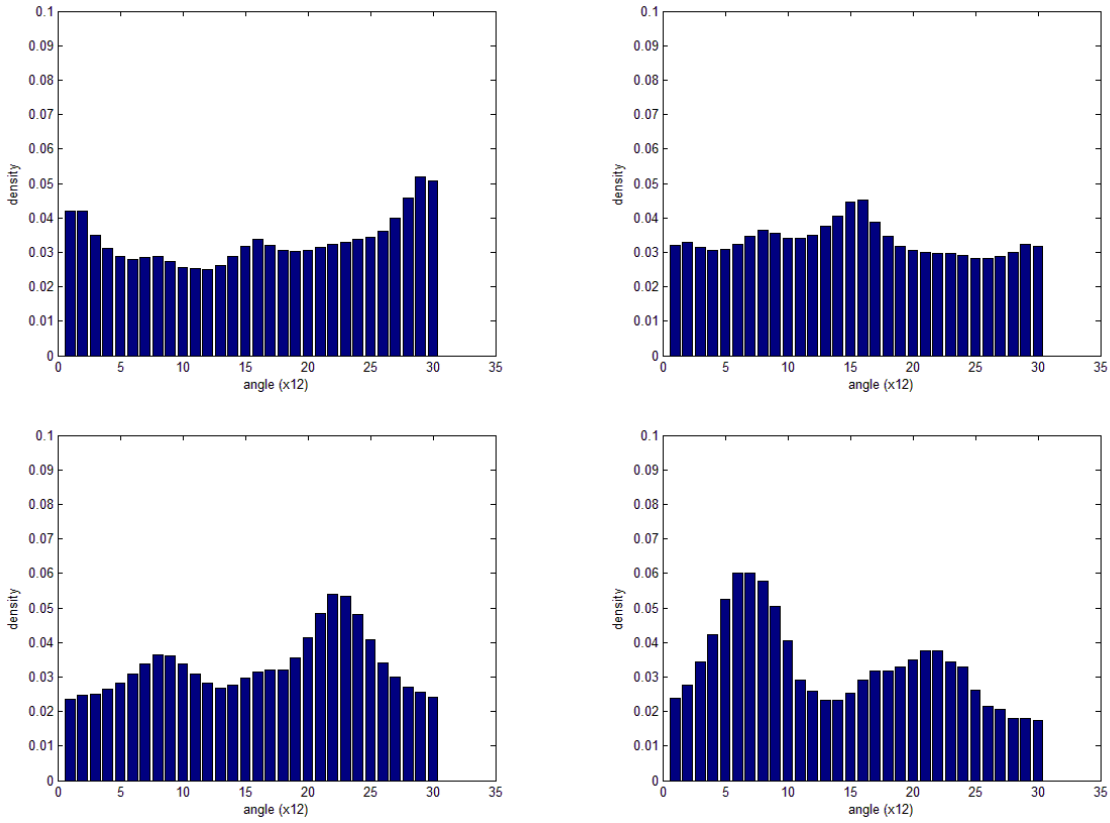

(d) Histograms with 30 bins

FIGURE 5. Histograms for the four different motion models (pan left, pan right, tilt up and tilt down) of the falsified faces with various number of bins

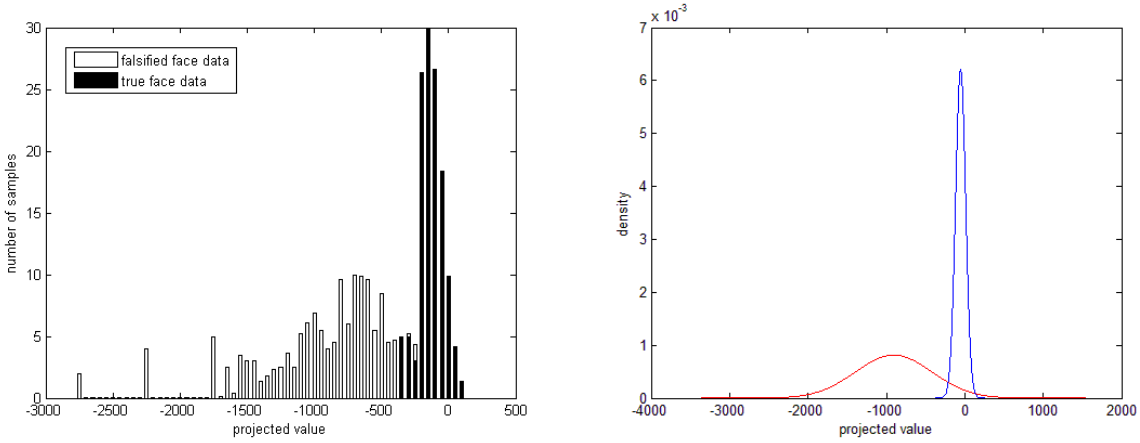

(a) (b)

FIGURE 6. Distribution of test data projected onto the LDA training space

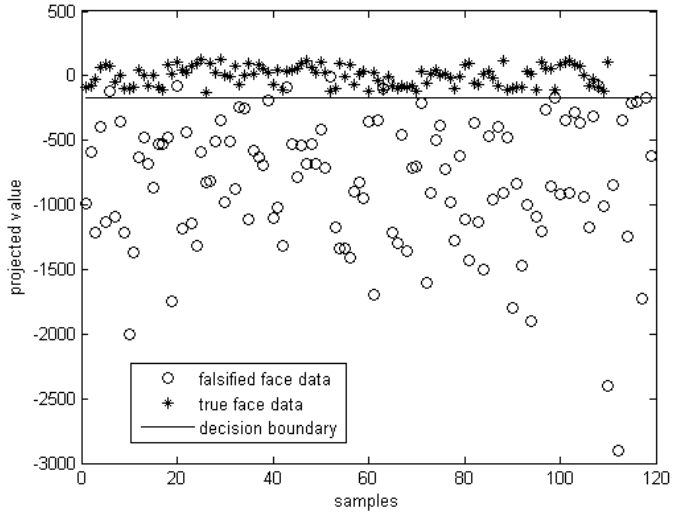

FIGURE 7. Projected test data for restricted face motions and decision boundary

TABLE 3. Detection of falsification using different numbers of frames per sample with restricted face motions using LDA and Bayesian classifier-based detection scheme

Number of Frames	Falsified Faces (Positive Samples)	True Faces (Negative Samples)	True Positive	True Negative	False Positive	False Negative	Precision	Recall
5	141	132	139	125	7	2	95.21%	98.58%
6	119	109	116	104	5	3	95.87%	97.48%
7	99	96	94	93	3	5	96.90%	94.95%
8	87	83	86	80	3	4	96.63%	98.85%
9	76	73	76	70	3	3	96.20%	100%

when optical flows from eight or nine frames are collected to form a sample. According to the above experiments, the precision rates achieved using detection scheme A are slightly higher than those achieved using detection scheme B. However, the recall rates of detection scheme B are much higher, so LDA and Bayesian classifier-based method is

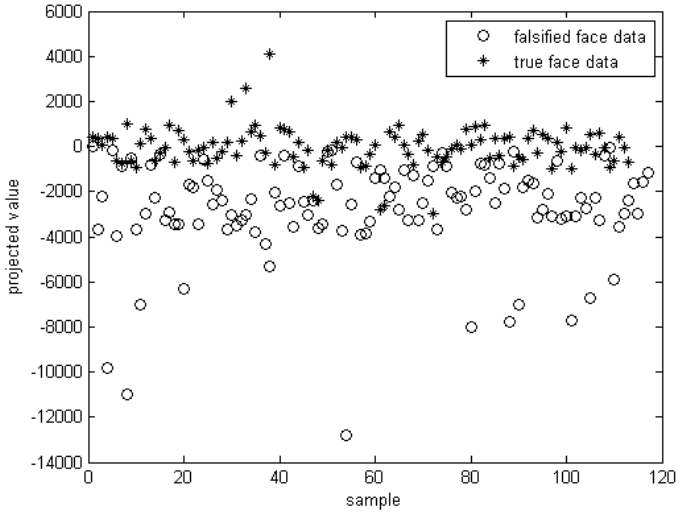

FIGURE 8. Projected test data for arbitrary face motions

TABLE 4. Detection of falsification using different numbers of frames per sample with arbitrary face motions using LDA and Bayesian classifier-based detection scheme

Number of Frames	Falsified Faces (Positive Samples)	True Faces (Negative Samples)	True Positive	True Negative	False Positive	False Negative	Precision	Recall
5	139	130	109	119	11	30	90.83%	78.42%
6	116	109	89	100	9	27	90.82%	76.72%
7	100	93	81	83	10	19	89.01%	81.00%
8	86	81	77	73	8	9	90.59%	89.53%
9	78	72	70	63	9	8	88.61%	89.74%

TABLE 5. Falsification detection using from true face and cut photo/mask with arbitrary face motions using the detection scheme B

Falsified objects	Falsified Faces (Positive Samples)	True Faces (Negative Samples)	True Positive	True Negative	False Positive	False Negative	Precision	Recall
Mask	86	81	61	65	16	15	79.22%	70.93%
Cut photo	85	81	69	68	13	16	84.14%	81.18%

more favorable. Although the computational cost in training phase of detection scheme B is much higher than that of the histogram-based scheme, this issue is not serious since training can be performed offline. Moreover, the required testing time for histogram matching increases when the number of bins increases.

An additional test is carried out. As shown in Figure 9, subjects wore a curved photograph or a mask on their faces. The main difference between the motion of true face and that of a photograph is related to their shapes. However, a mask or a curved photograph has a different shape or structure from a flat photograph. The difference is related to both the shape of the falsified face and the material on which the photograph is printed. Table 5 tabulates the results of classifying true faces and the cut photograph/mask. Five sequences of mask and cut photographs are used in this experiment. Detection scheme B is adopted with nine frames of optical flow field to form the feature vector. Although

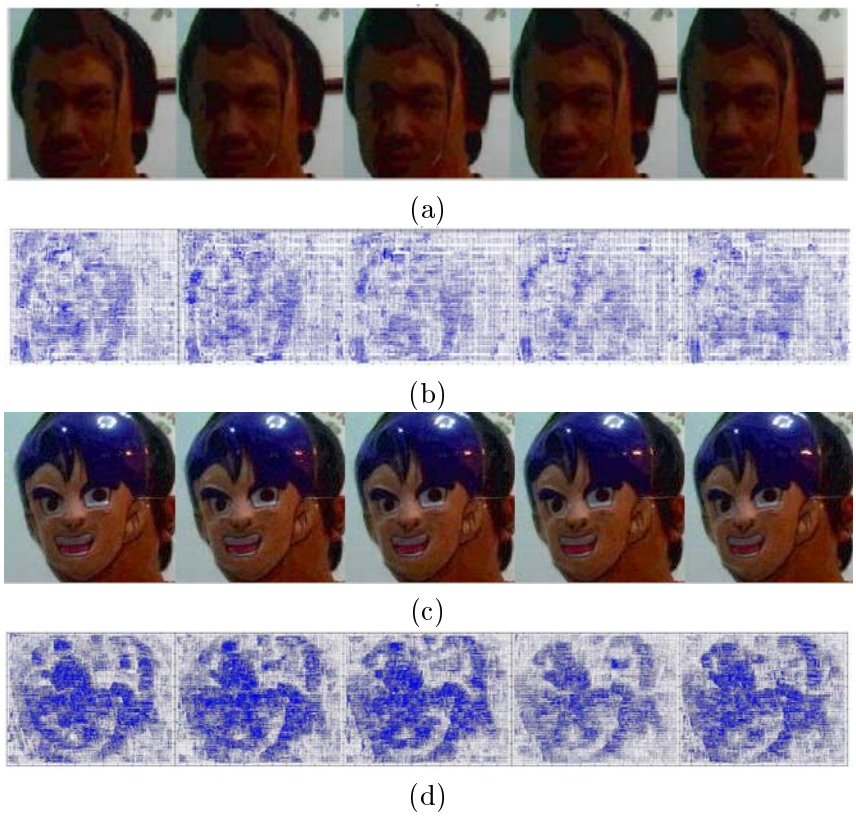

FIGURE 9. Example of different falsification objects. (a) Frames of curved photograph and (b) corresponding optical flow fields, (c) frames of mask and (d) corresponding optical flow fields.

some of the optical flow fields of the cut photograph are highly similar to those of the true face, the flow field across a short period is still different.

5. **Conclusions.** The falsification of human faces increasingly presents a challenge to face recognition and verification systems. A simple falsification scheme using photographs of faces can fool verification systems that use only static facial information. This paper proposes a system for distinguishing true faces from falsified faces according to information about their dynamic information obtained using the IDA optical flow method. The IDA optical flow method integrates multiple image frames so that the flow field is both temporally and spatially constrained simultaneously. The advantages of this method include increased smoothness and numerical stability. The estimated optical flow fields of true faces and falsified faces with face photographs are highly discriminative, especially when the system specifies the face motions that users must perform. This work compares two different detection schemes. The first detection scheme converts the flow estimation results into polar components and uses histogram matching to detect falsification. The second scheme projects the dense optical flow field across a short period into an optimal subspace using LDA and utilizes a Bayesian classifier to perform classification. LDA and Bayesian classifier-based detection scheme is better in terms of stability and recall rates. Experimental results show that the proposed system can successfully distinguish true face from falsified faces with satisfying accuracy, especially when user motions are restricted.

Acknowledgment. The authors would like to thank the National Science Council of Taiwan, for financially supporting this research under Contract No. 100-2221-E-238-014-.

Ted Knoy is appreciated for his editorial assistance. The authors also gratefully acknowledge the helpful comments and suggestions of the reviewers, which have improved the presentation.

REFERENCES

[1] A. Tefas, C. Kotropoulos and I. Pitas, Face verification using elastic graph matching based on morphological signal decomposition, *Signal Processing*, vol.82, no.6, pp.833-851, 2002.

[2] T. Hirayama, K. F. Lew, Y. Iwai and M. Yachida, Face detection and facial personation prevention by using infrared images, *SICE Annual Conference*, vol.1, pp.461-465, 2004.

[3] T. Tsuda, K. Yamamoto and K. Kato, A proposal of the distinguish technique between a real person and a photograph, *IEEE International Conference on Automatic Face and Gesture Recognition*, pp.391-396, 2004.

[4] S. Fazekas and D. Chetverikov, Analysis and performance evaluation of optical flow features for dynamic texture recognition, *Signal Processing: Image Communication*, vol.22, no.7-8, pp.680-691, 2007.

[5] P. Kruizinga and N. Petkov, Optical flow applied to person identification, *Proc. of the EUROSIM Conference on Massively Parallel Processing Applications and Development*, pp.871-878, 1994.

[6] X. Liu, T. Chen and B. V. K. V. Kumar, On modeling variations for face authentication, *Proc. of the 5th IEEE International Conference on Automatic Face and Gesture Recognition*, pp.369-374, 2002.

[7] L. F. Chen, H. Y. M. Liao and J. C. Lin, Person identification using facial motion, *Proc. of IEEE International Conference of Image Processing*, pp.7-10, 2001.

[8] B. K. P. Horn and B. G. Schunck, Determining optical flow, *Artificial Intelligence*, vol.17, pp.185-203, 1981.

[9] B. D. Lucas and T. Kanade, An iterative image registration technique with an application to stereo vision, *Image Understanding Workshop*, pp.121-130, 1981.

[10] J. D. Kim and S. K. Mitra, A local relaxation method for optical flow estimation, *Signal Processing: Image Communication*, vol.11, no.1, pp.21-38, 1997.

[11] J. D. Kim and J. Kim, Effective nonlinear approach for optical flow estimation, *Signal Processing*, vol.81, no.10, pp.2249-2252, 2001.

[12] A. Bruhn, J. Weickert and C. Schnörr, Lucas/Kanade meets Horn/Schunck: Combining local and global optic flow methods, *International Journal of Computer Vision*, vol.61, no.3, pp.211-231, 2005.

[13] J. R. Bergen, P. J. Burt, R. Hingorani and S. Peleg, A three-frame algorithm for estimating two-component image motion, *IEEE Transactions on Pattern Analysis and Machine Intelligence*, vol.14, no.9, pp.886-896, 1992.

[14] H. Shariat and K. E. Price, Motion estimation with more than two frames, *IEEE Transactions on Pattern Analysis and Machine Intelligence*, vol.12, no.5, pp.417-434, 1990.

[15] M. Irani, Multi-frame correspondence estimation using subspace constraints, *International Journal of Computer Vision*, vol.48, no.3, pp.173-194, 2002.

[16] R. O. Duda, P. E. Hart and D. G. Stork, *Pattern Classification*, 2nd Edition, Wiley-Interscience, 2001.

[17] C. M. Wang, C. C. Yu, H. Y. Cheng, K. C. Fan and F. Y. Hsieh, Distinguishing face falsification from true faces based on enhanced optical flow information, *IEEE International Symposium on Circuits and Systems*, Taiwan, 2009.

[18] C. M. Wang, K. C. Fan and C. T. Wang, Estimating optical flow by integrating multi-frame information, *Journal of Information Science and Engineering*, vol.24, no.6, pp.1719-1731, 2008.

[19] C. Xu, Face recognition based on enhanced supervised neighborhood preserving projection, *ICIC Express Letters*, vol.5, no.12, pp.4277-4282, 2011.

[20] M. Qi, J. Dai, Y. Shi and J. Kong, Video hiding method based on regression and visual attention model for secure face identification, *ICIC Express Letters*, vol.5, no.10, pp.3701-3706, 2011.

[21] J.-B. Li, Nonparametric kernel discriminant analysis for face recognition under varying lighting conditions, *ICIC Express Letters*, vol.4, no.3(B), pp.999-1004, 2010.